

PET for cerebrovascular disease: status and limitations

Vesna Sossi¹

Department of Physics and Astronomy, University of British Columbia

Vancouver, B.C., Canada

E-mail: vesna@phas.ubc.ca

The high resolution research tomograph (HRRT) is currently the most complex human brain scanner due to its ability to detect the gamma depth of interaction in the crystal, its octagonal geometry, and the large number of crystals (119,808) leading to approximately 4.5×10^9 possible lines of response (LORs). The scanner has a spatial resolution of $\sim (2.5\text{mm})^3$ and a sensitivity of $\sim 6\%$ and it thus provides an unprecedented wealth of spatial information. It is capable of very high acquisition count rates ($\sim 2.2 \times 10^6$ coincidence counts/sec) and is thus well suited for imaging tracers labelled with short lived radionuclides typically used in the study of cerebrovascular disease. Such performance comes at the cost of an increased hardware complexity that requires dedicated development of software tools and algorithms capable of dealing with large data sets, a highly variable number of acquired counts and count rates and some hardware instabilities. A summary of the performance highlights and associated limitation is presented.

*Frontiers in Imaging Science: High Performance Nuclear Medicine
Imagers for Vascular Disease Imaging (Brain and Heart)
Istituto Superiore di Sanita', Rome, Italy
13-14 November, 2006*

¹ Speaker

1. Introduction

The high resolution research tomograph (ECAT HRRT- Siemens, previously CTI PET systems) is one of the most complex existing Positron Emission Tomographs (PET) [1,2]. It is the only human size tomograph with a resolution of approximately 2.5 mm (axially and transaxially) and a phoswich detector, which employs two crystal materials with different decay times for γ depth of interaction (DOI) determination by pulse shape discrimination. The two 1 cm thick detector layers are made of cerium-doped lutetium-yttrium oxyorthosilicate (LSO, $\text{Lu}_2\text{SiO}_5\text{:Ce}$) and cerium doped lutetium-yttrium oxyorthosilicate ($\text{Lu}_{0.6}\text{Y}_{1.4}\text{SiO}_5\text{:Ce}$, i.e. 70% YSO and 30% LSO) with decay times of 43-44 ns and 53 ns, respectively. The lutetium in the crystal contains 2.6% ^{176}Lu , which is a β -emitter, thus providing a natural, low level constant radiation background ($t_{1/2} \sim 10^{10}$ yr). The photomultiplier (PMT) quadrant sharing detector design requires the overall 119,808 $2.2 \times 2.2 \times 10 \text{ mm}^3$ detectors of the 3D only scanner to be assembled in planar detector heads.

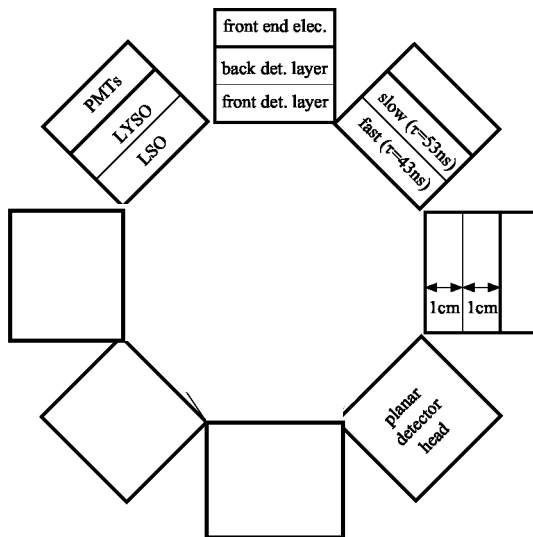


Figure 1. Physical layout of the HRRT scanner. Each head has 9 x 13 detector blocks, where each block is comprised by two layers of 8 x 8 crystals.

This design introduces small gaps between detector heads (figure 1), which preclude uniform sampling of the field of view (FOV). The FOV measures 25 cm in the axial and 31.2 cm in the trasaxial direction with a resulting slice thickness of 1.2 mm. Transmission scans, used to determine attenuation correction factors, are performed with a ^{137}Cs point source (662 keV γ -emitter, $t_{1/2} = 30.2$ yr). The total number of crystals allows for approximately 4.5×10^9 lines of reponse (LORs), i.e. possible detector pairs along which a coincident event consisting of a simultaneous detection of two γ rays, can be detected. The effects of the increased resolution achieved as a consequence of smaller detector size and high number of LORs is clearly visible

in figure 2 showing a ^{18}F -fluorodeoxyglucose (FDG) image obtained from a 30 min scan. However such improved performance is obtained at a cost of a much increased hardware and software complexity: the combination of the hardware structure and the large number of possible LORs presents new challenges at many different levels: hardware setup, data processing and image reconstruction. These challenges are particularly demanding in the realm of dynamic scanning, where accurate data quantification, i.e. proportionality between image count density and radioactivity concentration in the FOV, must be achieved in a situation of greatly varying acquisition count rates and number of acquired counts. Some of these challenges will be reviewed together with new advances in algorithm development that were stimulated by addressing these new challenges.

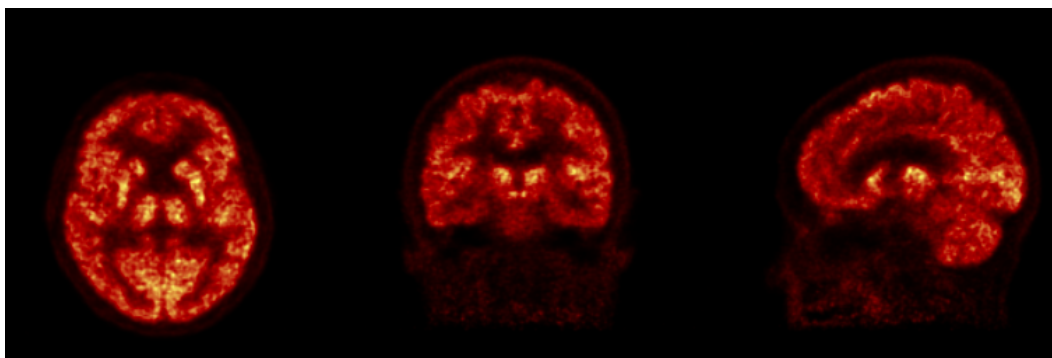


Figure 2. A transaxial, coronal and sagittal cross-section of an ^{18}F -fluorodeoxyglucose distribution image acquired over 30 min with a 5 mCi injection.

2. Hardware aspects

Two hardware aspects will be addressed: detector efficiency normalization and hardware stability issues. The γ detection efficiency of individual detectors or individual LORs is generally not completely uniform due to both intrinsic variations in crystal efficiency and to the geometric configuration of individual LORs. Such non-uniformity is corrected by normalization correction factors that bring each LOR to an average efficiency value and are determined from a scan of a uniform radioactivity source (normalization scan). For most scanners such detector uniformity correction factors tend to be fairly stable over a reasonably wide range of count rates. In the case of the HRRT the count rate dependence of the normalization correction factors is exacerbated by the DOI determination procedure. The DOI information is achieved using a pulse shape discrimination technique. In the presence of high count rates the pulse shape associated to an event can be altered by a ‘pile-up’ event, i.e. an event where a second γ ray interacts in the crystal and releases energy, while the system is integrating the energy released by the first γ ray (figure 3). This signal distortion results into a mis-assignment of the event to the back-end, slower crystal, thus altering the apparent crystal efficiency. The effect of a mismatch between the count rate at which the normalization scan and a regular emission scan are acquired can be observed in figure 4, where a normalization data set acquired at a count rate of $\sim 750,000$ cps was used to correct an emission scan of a cylinder filled with uniform radioactivity

concentration, acquired at a similar count rate ($\sim 650,00$ cps) and an emission scan of the same cylinder acquired at a lower count rate ($\sim 130,000$ cps). The high frequency artifact present in the mismatched situation is clearly visible.

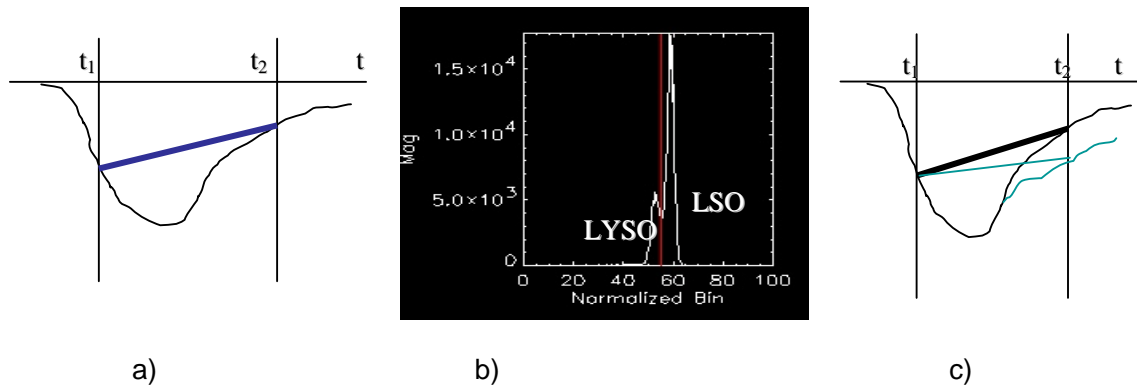


Figure 3. Pulse shape discrimination algorithm: a) the energy signal is sampled at two different time points and the slope of the solid line is taken to be an indicator of the scintillator decay time. b) slower scintillator (LYSO, back layer) has lower slope. c) a pile up event potentially reduced the observed slope thus forcing the assignment of the event to the back layer.

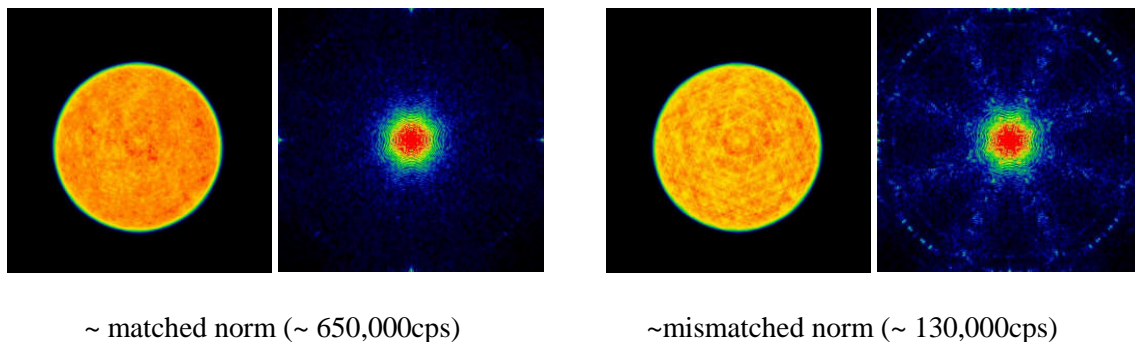
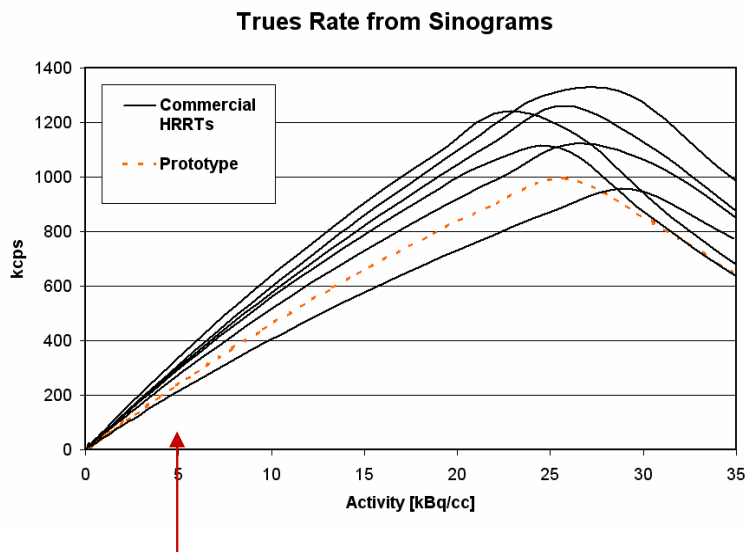


Figure 4. Image of a cylinder (and its 2D Fourier transform) filled with uniform activity in the case of the data corrected with a normalization scan acquired at a similar count rate (matched norm) and dissimilar count rate (mismatched norm).

An immediate solution to this problem is an attempt to match the count rates in the normalization scan with those of the emission scans and this can be done for most human studies where the amount of injected radioactivity is less than approximately 10 mCi. However this problem prompted the development of a count-rate dependent normalization where the apparent detector efficiency variation due to varying count rate is modelled into the correction factors [3]. Preliminary results are very promising. This is of particular importance, since the scanner is capable of much higher count rate than those observed after a 10mCi injection (fig. 5). Higher count rates would be indeed be obtained in a situation where a higher radioactivity

amount is injected; for example, when performing blood flow imaging with ^{15}O it is not unusual to administer 20-30 mCi as a bolus.

The second aspect discussed here is related to an observed hardware instability. It was observed that after each detector set-up (that is the procedure performed to equalize PMT gains) the observed count rate drops by approximately 5-10%. This effect was traced to a shift in the energy spectrum over time that causes more events where a γ ray undergoes Compton scattering to be detected in the predefined energy window (figure 6) [2]. The exact origin of this shift has not been identified to date and this problem is circumvented by performing frequent scanner sensitivity calibrations.



Assume a 10mCi injection in a 70 kg person.

Figure 5. True coincidence event count rate curves. Each curve was obtained from a different HRRT. The prototype refers to the first HRRT, which has a different crystal composition [4]. The arrow indicates the typical count rate obtained with a 10mCi in a 70 kg person.

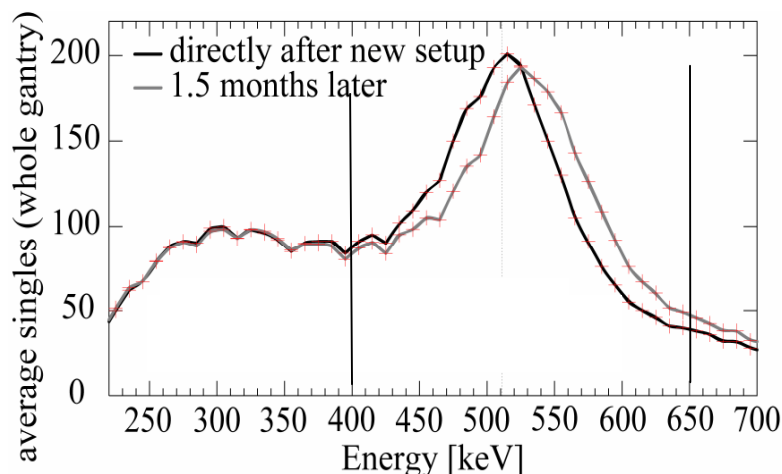


Figure 6. Energy spectrum observed immediately after scanner calibration (setup) and 1.5 months later. The acquisition energy window is 400-650keV. A shift to the left resulting into more accepted counts is observed 1.5 months after setector setup.

3. Software aspects

3.1 Reconstruction – non negativity bias.

Two main categories of reconstruction algorithms are used in the reconstruction of PET data: analytical and statistical reconstructions. The major advantage of the analytical reconstructions is that they are fast and linear, however they require uniform sampling. This is not the case for the HRRT due to the presence of gaps between detector heads. The statistical reconstruction algorithms, while able to model detector geometry and the random nature of the decay process, are not linear and generally do not perform in a robust fashion in a situation of a low number of counts.

When performing dynamic scanning, i.e. performing a series of temporally contiguous scans (time-frames), which allow to follow the tracer spatial distribution as a function of time, the number of acquired counts and the count rate vary significantly from frame to frame; for example, in a study with a typical 10mCi injection of a ^{11}C labelled dopaminergic tracer, often histogrammed into a 16 frame sequence, the count rate ranges from 20,000 cps to 400,000 cps and the number of events per frame from 2M to 100M. The duration of each frame is adjusted to optimally capture tracer kinetics, while tracer decay is the main source of variation in count rates. When performing data reconstruction care needs to be taken to eliminate random coincidences from the acquired data sets together with events where one of the two or both γ rays undergo Compton scattering: such events introduce a mis-identification of the source position and therefore detract from the quantitative accuracy of the final images. In the most simplistic approach statistical algorithms perform such corrections by direct subtraction of random and scattered events (random events are generally measured with a delayed coincidence window technique, while scattered events are determined using modeling techniques).

A very common iterative statistical reconstruction algorithm takes the form of typical ordered subsets maximum likelihood expectation maximization (OSEM) [5] and looks as follows:

$$\lambda_j^{m+1} = \frac{\lambda_j^m}{\sum_{i=1}^I p_{ij}} x \sum_{i=1}^I p_{ij} \left(\frac{y_i - r_i - s_i}{\sum_{b=1}^J p_{ib} \lambda_b^m} \right)$$

where λ_j is the estimated image count density in image voxel j , y_i is the number of total acquired event in the LOR i , and r_i and s_i are the number of scatter and random events in the same LOR, while p_{ij} is an elements of the system matrix (or sensitivity matrix) describing the probability that an event emitted in the image voxel j is detected along the LOR i .

An immediately apparent problem with this formulation of the algorithm is the fact that in a situation of low number of counts in the presence of high count rates (as is often the case in the first frames of a dynamic study) the numerator of the image update factor may become negative, since the estimate of the number of random events is obtained independently from the total number of acquired counts. At first a non-negativity constrain on the update factor was introduced, however this was found to cause a significant positive bias in the images [6]. This problem stimulated significant development in the image reconstruction area, which lead to the practical implementation of the currently most widely accepted reconstruction method, Ordinary Poisson-OSEM [7-9], where the images are reconstruted using the following expression:

$$\lambda_j^{m+1} = \frac{\lambda_j^m}{\sum_{i=1}^I p_{ij}} x \sum_{i=1}^I p_{ij} \left(\frac{y_i}{\sum_{b=1}^J p_{ib} \lambda_b^m + \bar{r}_i + \bar{s}_i} \right)$$

In this approach the random and scattered events are included into the image estimate and no subtraction is performed in the numerator. This algorithm requires a statistically reliable scatter and random estimate: since the scatter is generally estimated using model based scatter approaches, this condition was satisfied from the very outset [10]. The inclusion of random events into the image estimate however required the development of new variance reduction approaches[11-12], which have considerably improved the robustness of the reconstruction algorithm.

3.2 List mode reconstruction

Considering the high number of possible LORs in the HRRT, it frequently happens that the number of acquired events is lower than the number of LORs. Since the HRRT is capable of acquiring data in list mode, it is often advantageous to reconstruct the data directly from the list mode file as opposed to first assigning the data to sinogram bins. As a consequence several groups have explored list mode based reconstruction algorithms [6, 13-15] of which a particular implementation results into the following modifications of the expression listed above:

$$\lambda_j^{m+1} = \frac{\lambda_j^m}{\sum_{i=1}^I p_{ij}} \times \sum_{k=1}^N p_{ikj} \left(\frac{1}{\sum_{b=1}^J p_{ib} \lambda_b^m + \bar{r}_i + \bar{s}_i} \right)$$

Here the summation is performed over individual events (i_k) as opposed to being performed over LORs. An ideal situation would allow to switch between list mode and sinogram mode reconstruction algorithms depending on the number of events acquired in each frame. Developments in this direction are under way and preliminary results point towards feasible algorithms [16].

4. Patient motion

Given the high resolution capabilities of the HRRT, patient motion has a relatively greater impact on image degradation compared to other scanners. Patient motion monitoring and correction become thus of great relevance. Since PET studies often extend over one hour or more, complete immobilization of the patient head is not feasible. Although restraining devices that limit patient motion are generally used, there is often significant patient motion, especially when imaging patient with medical conditions [17]. Figure 7 shows the amount of motion detected with the Polaris motion tracking system averaged over typical frame durations for a healthy volunteer compared to the amount of motion detected over the same length of time when scanning a volunteer suffering from Parkinson's disease (PD). It can be observed that for the PD subject the magnitude of motion is greater than the resolution of the scanner.

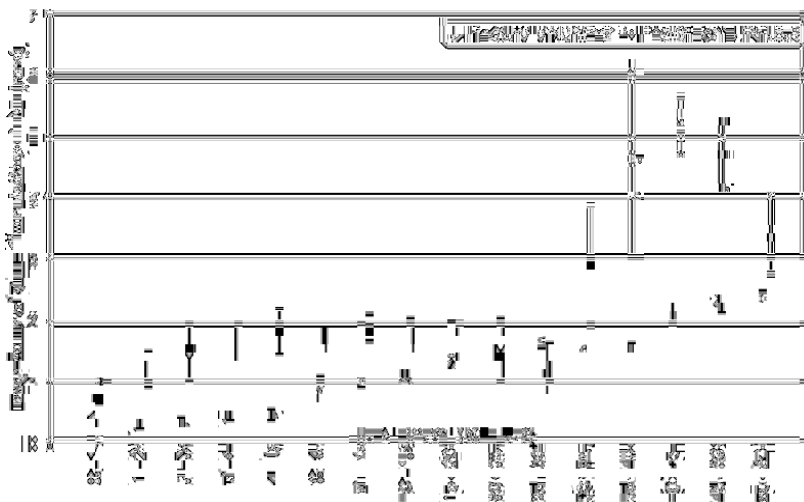


Figure 7. Amount of motion determined with the Polaris tracking system for a series of 5 minute intervals comprising a one hour long scanning session.

The Polaris tracking system is becoming the method of choice to monitor patient motion. When such information is synchronized with the scanner data acquisition, events can be corrected for motion essentially on-line [18-19]. Such correction relies on two critical steps. First, for each event one must keep track of the crystal pair that detected that particular event so that proper detector normalization factors are used. This can be performed directly on the acquired data. The second step is more subtle and requires the modification of the reconstruction algorithm. Considering that the HRRT has gaps, patient motion might cause an event that might be detected in a situation of no motion to exit the active FOV in the presence of motion and conversely an event that would not have been detected to hit the crystals. This implies that the detection sensitivity associated with each position in the object varies as a function of motion and thus the sensitivity matrix must be changed accordingly. Several approaches to motion correction are currently investigated [18-20]. Figure 8 shows a simulated data set, where a realistic amount of motion was introduced in the data, and compares the case where the data were (i) not motion corrected, (ii) motion corrected including proper LOR normalization only and (iii) motion corrected including proper LOR normalization factors and variations in the sensitivity matrix during reconstruction. Clear residual artefacts are visible when the the reconstruction algorithm does not account for variations in the sensitivity matrix.

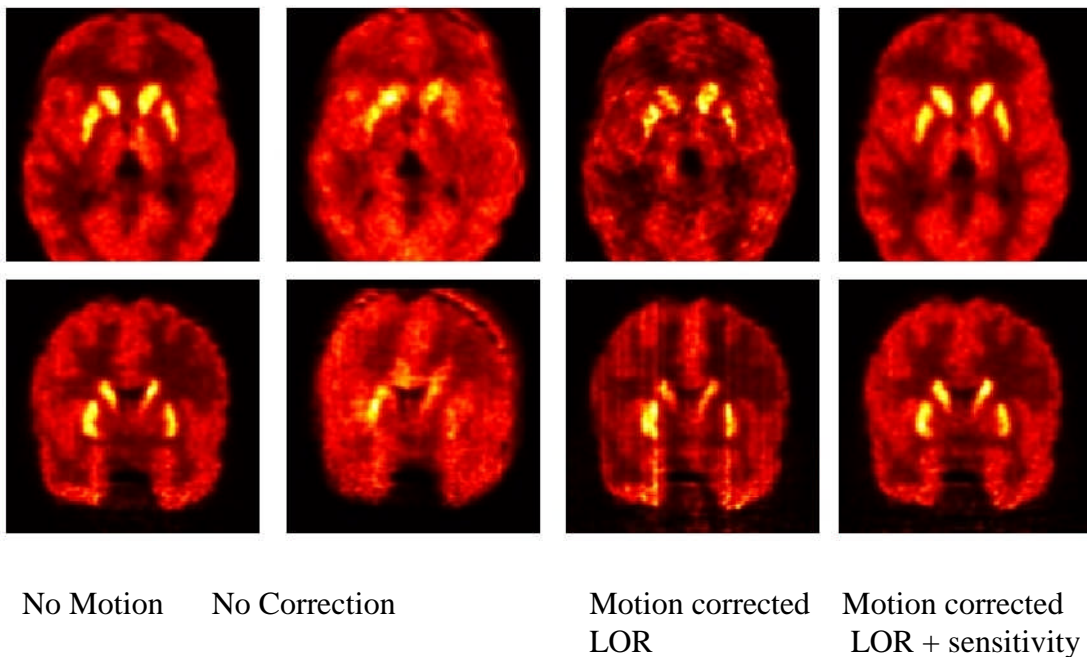


Figure 8. Simulated data set with no motion, realistic amount of motion and corrected with the motion correction procedures.

5. Image analysis

The HRRT large axial field of view and small slice thickness results into 207 imaging planes (figure 9). This provides a large amount of spatial detail, so that traditional region of interest (ROI) based analysis, where the analysis is limited to pre-identified structures of interest, might either not be practical or would not fully take advantage of the available information. Parametric approaches, where the biologically important parameters are calculated for each pixel, might be better suited to the analysis of such large data sets. Given the small image pixel size of the HRRT images, it is important to determine the influence of the statistical quality of the data on such parametric maps; it is infact known that different modelling approaches exhibit different sensitivities to noise in the data [21]. Finally methods such 4D imaging where kinetic parameters are extracted from the data directly during image reconstruction are becoming of increasingly higher interest [22].

6. Conclusion

In conclusion the HRRT has provided the PET brain imaging field with a scanner of unprecedented resolution and count rate capabilities. Such a scanner can be ideally suited for the investigation of cerebrovascular diseases, where administration of tracer with short lived radionuclides, such as ^{15}O results in high administered radioactivity amount. However due to its hardware complexity the HRRT is also a very high maintenance scanner, which requires frequent calibration and constant monitoring and fine tuning. On the other hand, its very complexity and required use for dynamic imaging stimulated the development and critical examination of many new algorithms, ranging from detector normalization to patient motion correction.

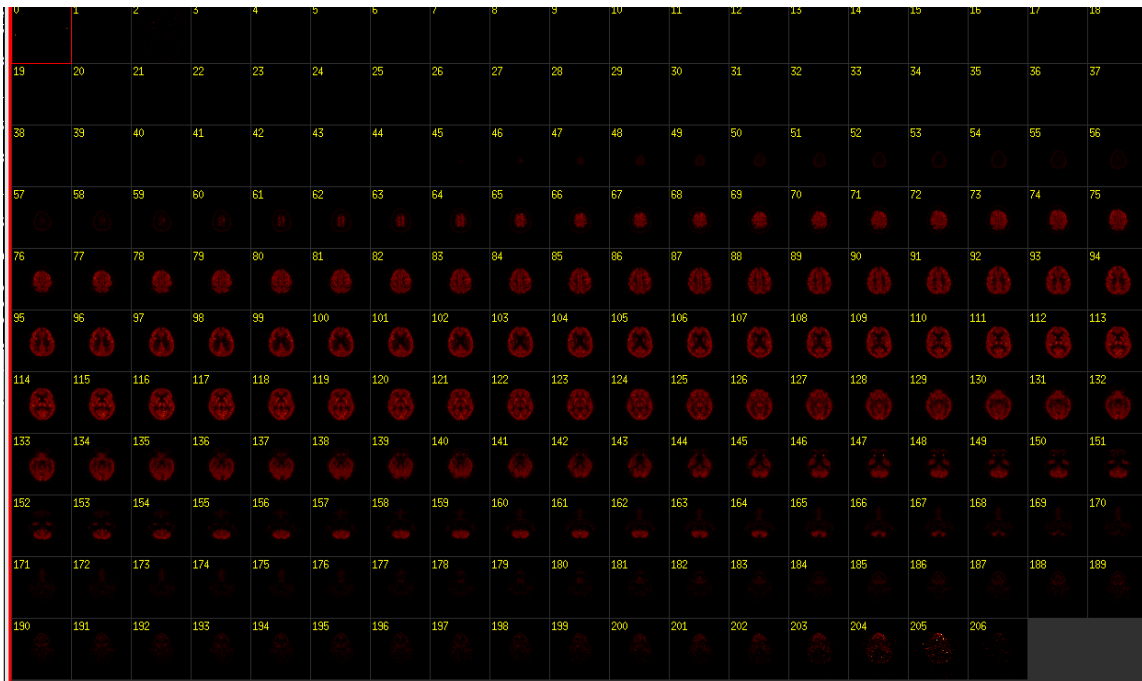


Figure 9. 207 HRRT transaxial image planes: FDG distribution images.

References

- [1] de Jong HW, van Velden FH, Kloet RW, Buijs FL, Boellaard R, Lammertsma AA. *Performance evaluation of the ECAT HRRT: an LSO-LYSO double layer high resolution, high sensitivity scanner*. Phys Med Biol. (2007) 52(5):1505-26
- [2] Sossi V, de Jong, H, Barker, WC et al., *The second generation HRRT - a multi-centre scanner performance investigation*, IEEE Nucl Sci Symp Conf Rec, (2005) 4 2195 - 2199.
- [3] Rodriguez M, Barker WC, Liow JS, Thada S, Chelikani S, Mulnix T, Carson RE. *Count rate dependent component-based normalization for the HRRT*. J Nucl Med. 47:197P, 2006
- [4] Wienhard K, Schmand, Casey ME et al., *The ECAT HRRT: Performance and first clinical application of the new high resolution research tomograph*, IEEE Trans. Nucl. Sci., (2002) 49: 104-110
- [5] Hudson H M and Larkin R S *Accelerated image reconstruction using ordered subsets of projection data* IEEE Trans. Med. Imaging (1994) 13(4):601 – 609
- [6] A Rahmim, M Lenox, A J Reader, C Michel, Z Burbar, T J Ruth and V Sossi *Statistical list-mode image reconstruction for the high resolution research tomograph* Phys. Med. Biol. (2004) 49 4239-4258
- [7] Politte DG and Snyder DL, *Corrections for Accidental Coincidences and Attenuation in Maximum-Likelihood Image Reconstruction for Positron-Emission Tomography*, IEEE Trans. Med. Imaging (1991) 10 (1): 82-89
- [8] Comtat C, Bataille F, Michel, C et al., *OSEM-3D reconstruction strategies for the ECAT HRRT*, IEEE Nucl Sci Symp Conf Rec (2004) 6:3492 - 3496
- [9] Rahmim A, Cheng JC, Blinder S, Camborde ML, Sossi V *Statistical dynamic image reconstruction in state-of-the-art high-resolution PET*. Phys Med Biol. (2005) 50(20): 4887-912
- [10] C. C. Watson, *New, Faster, Image-Based Scatter Correction for 3D PET*, IEEE Trans. Nucl. Sci., (2000) 47: 1587-1594
- [11] Barker, W.C. Liow, J.-S. Rodriguez, M. Shanthalaxmi Thada Iano-Fletcher, A.R.; Lenox, M.; Michel, C. Johnson, C.A. Carson, R.E. *Randoms estimation for list-mode reconstruction for the ECAT HRRT* IEEE Nucl Sci Symp Conf Rec (2004) 6:3510 - 3513
- [12] Byars, L.G. Sibomana, M. Burbar, Z. Jones, J. Panin, V. Barker, W.C. Jeih-San Liow Carson, R.E. Michel, C *Variance reduction on randoms from coincidence histograms for the HRRT*. IEEE Nucl Sci Symp Conf Rec (2005) 5:2622 - 2626

- [13] Parra L and Barrett HH, *List-mode likelihood: EM algorithm and image quality estimation demonstrated on 2-D PET*, IEEE Trans. Med. Imaging, (1998) 17 228-235
- [14] Reader A J, Ally S, Bakatselos F, Manavaki R, Walledge R, Jeavons A P, Julyan P J, Zhao S, Hastings D L and Zweit J; *One-pass list-mode EM algorithm for high-resolution 3-D PET image reconstruction into large arrays* IEEE Trans. Nucl. Sci. (2002) 49 693-9
- [15] Carson RE, Barker WC, Liow JS, Yao R, Thada S, Zhao Y, Iano-Fletcher A, Lenox M, Johnson CA, *List-mode reconstruction for the HRRT*, J Nucl Med, (2004) 45:105P
- [16] Cheng K, Rahmim A, Blinder S, Camborde M-L, Raywood K, and Sossi V, *A scatter-corrected list-mode reconstruction and a practical scatter/random approximation technique for dynamic PET imaging* (2007) Phys. Med. Biol. **52** 2089-2106
- [17] Dinelle K, Blinder S, Cheng J-C, et al., *Investigation of Subject Motion Encountered During a Typical Positron Emission Tomography Scan* IEEE Nucl Sci Symp Conf Rec (2006) in press
- [18] Carson, R.E.; Barker, W.C.; Jeih-San Liow; Johnson, C.A *Design of a motion-compensation OSEM list-mode algorithm for resolution-recovery reconstruction for the HRRT*, IEEE Nucl Sci Symp Conf Rec (2003) 5: 3281 - 3285
- [19] Rahmim, A. Bloomfield, P. Houle et al., *Motion compensation in histogram-mode and list-mode EM reconstructions: beyond the event-driven approach*; IEEE Trans Nucl Sci (2004) 51 (5.2):2588 – 2596
- [20] Buhler, P. Just, U. Will, E. Kotzerke, J. van den Hoff, J. *An accurate method for correction of head movement in PET*; IEEE Trans Med imaging (2004) 23 (9):1176 – 1185
- [21] Sossi V, Blinder S, Dinelle K et al., *Comparison between the ROI based and pixel based analysis for neuroreceptor studies performed on the high resolution research tomograph (HRRT)*, IEEE Nucl Sci Symp Conf Rec (2006) in press
- [22] Reader AJ, Sureau FC, Comtat C, Trebossen R, Buvat I. *Point estimation of dynamic PET images and temporal basis functions using fully 4D ML-EM*. Phys Med Biol. (2006) 51(21):5455-74